International Conference on Space Optics—ICSO 2000

Toulouse Labège, France

5–7 December 2000

Edited by George Otrio

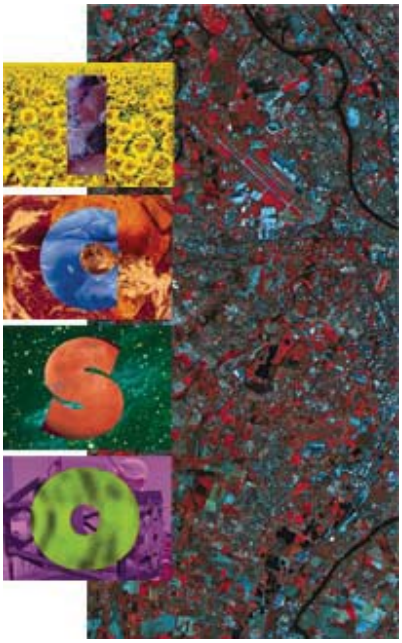

Integrated optics interferometer for high precision displacement measurement

Dominique Persegol, Virginie Collomb, Vincent Minier

International Conference on Space Optics — ICSO 2000, edited by George Otrio, Proc. of SPIE Vol. 10569
105691H · © 2000 ESA and CNES · CCC code: 0277-786X/17/$18 · doi: 10.1117/12.2307929

INTEGRATED OPTICS INTERFEROMETER FOR HIGH PRECISION DISPLACEMENT MEASUREMENT.

Dominique PERSEGOL, Virginie COLLOMB*, Vincent MINIER.

Groupement d'Electromagnétisme Expérimental et d'Optoélectronique (GeeO).
13 chemin du vieux chêne, 38240 Meylan, France. Tel. (33) 4 76 04 05 26, Fax (33) 4 76 04 79 55, Email : dominique.persegol@geeo.com.
**Laboratoire d'Electromagnétisme de Micro-ondes et d'Optoélectronique (LEMO), ENSERG, 23 avenue des Martyrs, BP257, 38016 Grenoble cedex, France.*

ABSTRACT - We present the design and fabrication aspects of an integrated optics interferometer used in the optical head of a compact and lightweight displacement sensor developed for spatial applications.
The process for fabricating the waveguides of the optical chip is a double thermal ion exchange of silver and sodium in a silicate glass. This two step process is adapted for the fabrication of high numerical aperture buried waveguides having negligible losses for bending radius as low as 10 mm.
The optical head of the sensor is composed of a reference arm, a sensing arm and an interferometer which generates a one dimensional fringe pattern allowing a multiphase detection. Four waveguides placed at the output of the interferometer deliver four ideally 90° phase shifted signals.

1. INTRODUCTION

Interferometers are widely used to provide high resolution displacement measurements over long distances. The integration of interferometers on optical chips leads to the fabrication of compact structures adapted to environments where the size and weight of sensors are important considerations. Moreover, the principle of fabrication of integrated optical circuits provides an inherent permanent alignment of the optical circuits and therefore a natural insensitivity to vibrations [Fues 93].

Displacement sensors are composed of a wavelength stabilized laser diode, an optical head and a processing electronics. Depending on the application, these different elements can be associated for example by hybridization on the same board, or the optical head can be separated from the laser source and/or the electronic elements by optical fibers.
Regarding the optical head a careful design of the integrated circuits is required in order to optimize the quality of the interferometer as well as the optical power balance between the reference and measuring arms. These parameters are indeed playing a significant role in the contrast level of the interference pattern and therefore in the accuracy of the measurement.

2. DESCRIPTION OF THE SENSOR HEAD

The basic components of the sensor head are the reference arm, the measuring arm and the interferometer. Fig. 1 shows the design of the sensor head and its environment, established within the frame of a collaboration with CSO Mesure [Poup 00]. In the measuring arm a movable mirror intercepts the free beam coupled out of the chip.

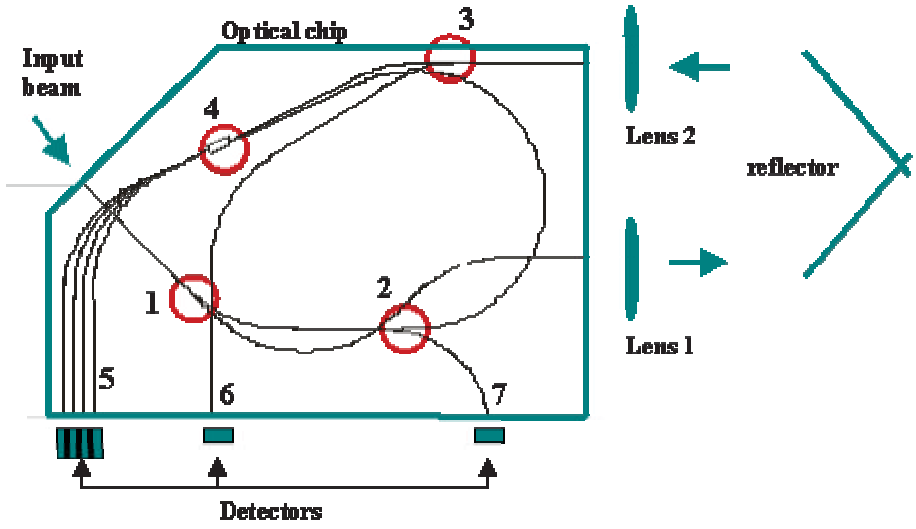

Fig. 1 : Design of the sensor head and its environment.

Light from a remote laser diode is fed to the integrated optical glass chip with a single mode fiber. The beam injected in the input waveguide of the sensor is divided between the measuring and reference arms by a coupler (element 1 in Fig. 1).
An integrated loop in the reference arm acts as a mirror. In the other branch the guided light is coupled out of the glass onto the measuring path as a parallel beam with a first lens, after its reflection on a corner cube the beam is collimated in the chip with a second lens.
Two additional asymmetric couplers (elements 2 and 3 in Fig. 1) situated in the reference and measuring arms are used to couple a small fraction of light in waveguides 6 and 7.

3. THE INTEGRATED INTERFEROMETER

In the interferometric head, the reference and the sensing waveguides approach with a small angle to one another while adiabatically widened as shown in Fig. 2. Because of the small half-angle ($\theta = 0.15°$) of the tapers the power carried in the fundamental mode of the input waveguide is entirely coupled to the fundamental local mode along the entire length of the structure.

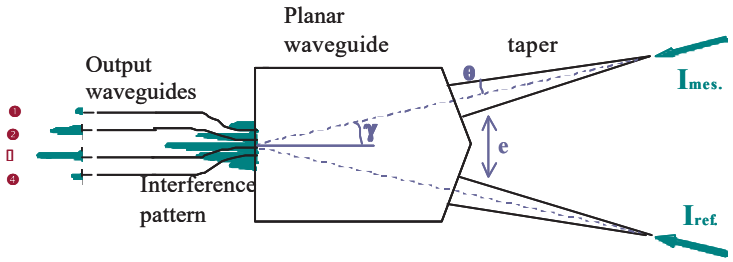

Fig. 2 : Design of the interferometer head (element 4 in fig. 1).

During propagation in the planar waveguide, the two beams continue to approach with a small half-angle of inclination between their axes (γ = 1.04°). In the intersection zone, the two beams overlap completely and produce a one-dimensional interference pattern in the x direction [Scha 94].

Fig. 3a shows the result of a simulation performed with a Beam Propagation Method (BPM) program using a taper length of 7.3 mm, the planar waveguide being 1.652 mm long and 100 µm wide. The light coming from the two single mode waveguides is seen to widen in the tapers and the overlap of the two beams in the planar waveguide produces the interference patterns. Fig. 3b represents a cross section of the interference pattern (along the lateral x direction) at the output of the planar region.

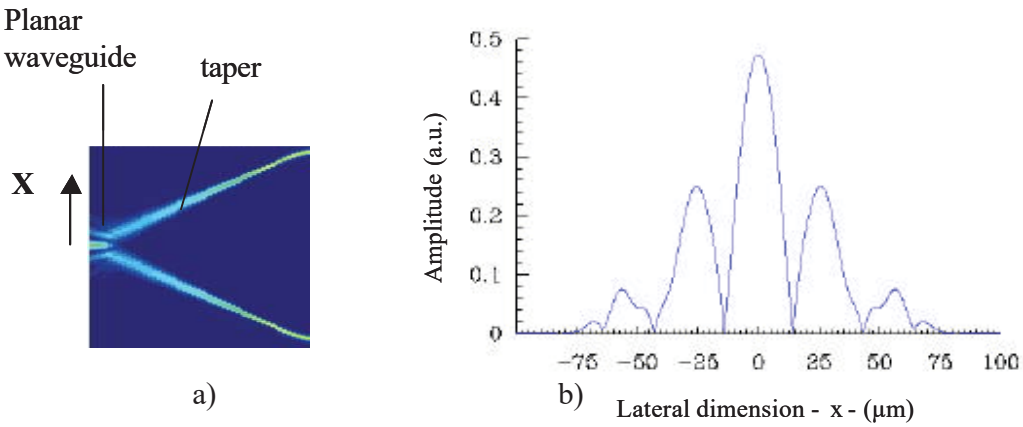

Fig. 3 : BPM simulation of the multimode interference pattern:
a) top view and b) cross-sectional view of the interference pattern (along - x -).

The separation between taper extremities (e = 20 µm) is large enough in order to prevent coupling of the beams before they enter the planar section. The interference pattern is limited by a Gaussian envelope (according to an approximation) given by the spatial distribution of the two beams coming from the tapers and after their propagation in the planar region.

The maximum of intensity of the interference pattern is centered on the axe of the planar waveguide (as shown in Fig. 3b) when the phase difference between the guided modes of the reference and measuring arms is equal to zero ($\varphi = 0 \pm 2k\pi$). A relative phase variation between the two modes will shift the interference pattern laterally.

Four output channel waveguides placed in the focal plane of the interference pattern sample the latter. The relative position of the four integrated waveguides is chosen in order to provide four ideally 90° phase shifted optical signals which are transmitted to four photodetectors (Fig. 1) where they are processed by a suitable electronic treatment to display the displacement of the reflector.

The interference pattern at the output of the planar waveguide can be expressed by:

$$I(x) = I_M(x)\,(1 + \cos(\quad + 2\pi\,(x/i))$$

where $I_M(x)$ is the envelope of the interference pattern which depends on the intensity of the two Gaussian beams (the dependence along y is not considered in the following expressions):

$$I_r(x) = I_{ro} \exp(-2x^2/\sigma^2) \quad \text{and} \quad I_m(x) = I_{mo} \exp(-2x^2/\sigma^2)$$

For small values of the half-angle between the axes of the two tapers, $I_M(x)$ can be written:

$$I_M(x) = I_{Mo} \exp (-2x^2 / \sigma^2)$$

Where σ is the half-width at $1/e^2$ of the Gaussian envelope of the interference pattern, i the spatial periodicity of the fringes given by the distance between two successive minima and the phase difference between the two beams.
This phase difference depends on the position of the reflector according to the term:

$$= (2 /) 2 n_e x$$

where = 1.55 µm is the wavelength of the source, n_e the effective index of the guided mode and x the displacement of the reflector.

Fig. 4 shows the evolution of the interference pattern for a 0.2 µm variation of the position of the reflector.

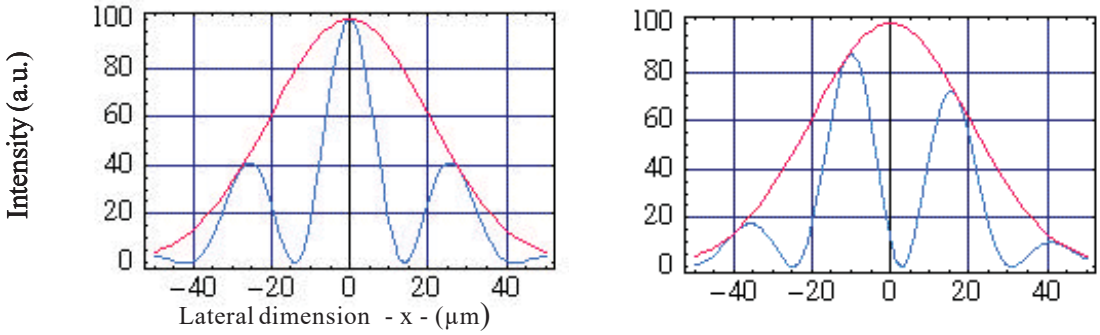

Fig. 4 : Theoretical evolution of the interference pattern for equal beam intensities ($I_{ro} = I_{mo}$) versus the reflector position: a) position of reference, b) displacement of 0.2µm.

A careful choice of the distance between the 4 output waveguides allows to sample the interference pattern with the desired phase differences. They are positioned at the following x-coordinates: -31.5, -10.5, 10.5 and 31.5 µm with respect to the center of the planar waveguide in order to generate four 270° phase shifted signals. A 21 µm spacing between two adjacent channel waveguides prevents coupling and generates a relative phase lag of –90°. After their electronic conversion, the amplitudes of the 4 signals are equalized and the amplitudes of channels 1 and 3 (resp. 2 and 4) are subtracted in order to suppress the DC offset voltage which appears when the intensities in the reference and measuring arms are not balanced [Lang 98].

4. FABRICATION OF THE SENSOR HEAD

The ion exchange technology is a widely used process to fabricate low loss integrated optical waveguides [Rama 94].

4.1. Process steps

The integrated circuits of the sensor head are fabricated by a two step ion exchange process in a silicate glass substrate. The original mask design is copied by photolithography onto the glass wafer previously coated with a metal and a photoresist layer. After development of the insolated photoresist and etching of the metal layer the original mask design is transferred into the metal mask.

During the first step of the process, the glass substrate is immersed into a molten salt bath which contains doping silver ions. An exchange occurs through the openings of the mask between the metallic ions of the bath and the sodium ions of the glass. This local substitution of ions with different polarizabilities and radius leads to an increase of the refractive index in the exchanged regions of the wafer.

During the second step of the process, the metal mask is removed and the wafer is immersed into a molten salt bath which contains sodium ions. The back-interdiffusion of sodium permits to rebuilt the original structure of the glass near the surface. Since the substitution is not complete, silver ions are still present into the glass with a maximum of concentration a few microns below the surface. After exchange, the circuits are endface-polished.

4.2. Chip dimensions

As described earlier (Fig. 1), the bending radius of the integrated waveguides should be kept as small as possible to minimize the dimensions of the integrated loop in the reference arm. One main advantage of double thermal ion exchange is that this process is adapted for the fabrication of low loss integrated structures with large refractive index variations between the guide profile and the substrate.

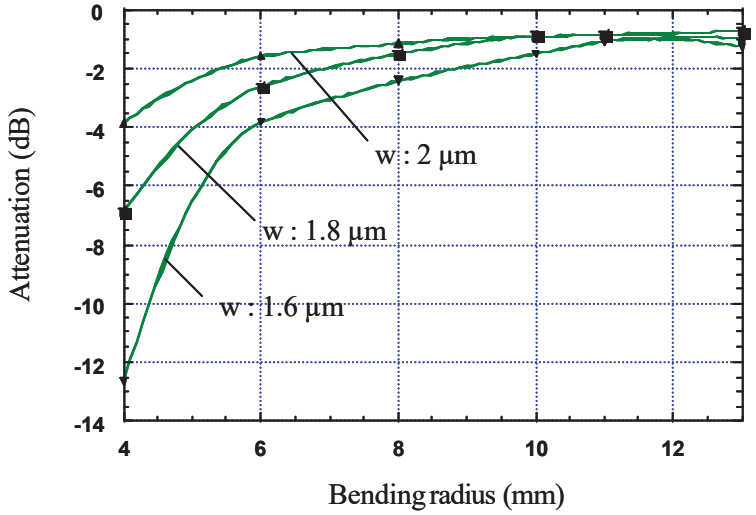

Fig. 5 : Evolution of the insertion losses versus bending radius.
w : opening of the test mask.

We have measured the evolution of the waveguide losses for various bending radius with a test mask containing three series of guides with different widths (w = 1.6 to 2 µm). The guide design consisting of two assembled S-shaped bending structures. In this configuration, the straight input and output waveguide sections are aligned, which makes the characterization of the components easier.
The mode confinement is dependent of the amount of exchanged species in the guide: the larger the mask opening, the more important the doping. Fig. 5 shows that the intensity of optical signals carried by waveguides having initial mask openings larger than 1.8 µm is not affected by bending radius larger than 10 mm. All the waveguides are single mode at 1.55 µm.
A 1.9 µm mask opening width and a minimal bending radius of 10 mm were chosen in the design of the sensor head.

4.3. Characterization of the couplers

Coupler 1 of the sensor head is used to split the input light between the two arms of the device. Couplers 2 and 3 (in Fig. 1) are used as taps in order to inject a small amount of light in the photometric branches of the device.

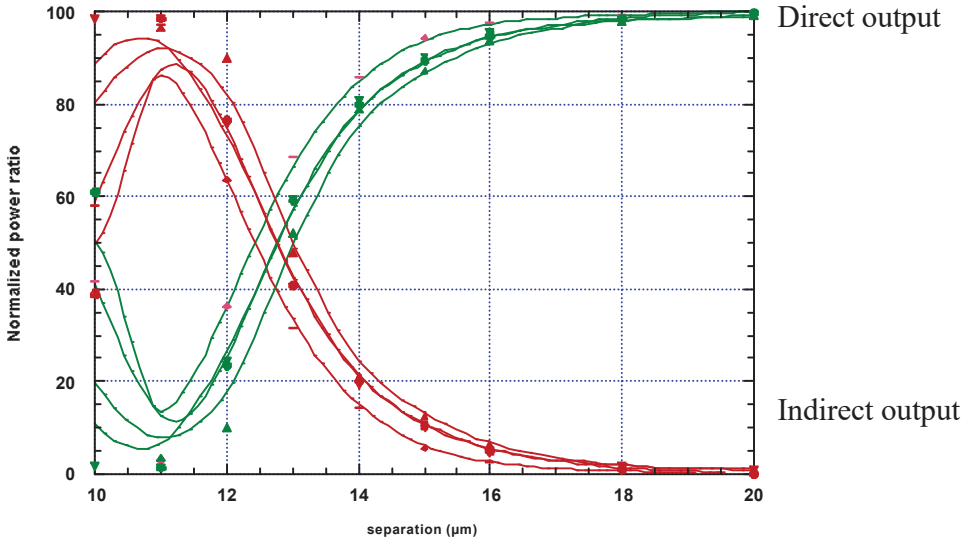

Fig. 6 : Intensity splitting in the output arms of the couplers as a function of the waveguide spacing (axis to axis), λ = 1.55 µm.

Directional couplers with various inter-guide distances were tested. Fig. 6 gives the evolution of the intensity distribution in the output arms of the structure versus the waveguide separation. The graph shows the dispersion obtained with four series of couplers fabricated on different chips with the same process parameters. As it can be seen, the output guides are totally isolated from each other for separation distances larger than 20 µm. This measurement justifies the choice described earlier of the four waveguide spacing (21 µm) at the output of the interferometer head.

4.4. Characterization of the integrated interferometer

The experimental observation of the interference pattern is performed by cutting the integrated interferometer at the output of the planar waveguide. We used a test mask composed of an integrated Y-junction linked to an interferometer in order to balance the coupled intensity in the two arms of the structure. The beam at the output of the device is focused with a magnifying microscope objective on an IR camera.

Fig. 7a represents an image of the experimental interference pattern recorded on the monitor screen. As can be seen the measured intensity profile (Fig. 7b) shows a good contrast between the bright an dark levels of the sampled image.

The fringe spacing measured between two successive minima on three samples is i = 28.1 $\pm$ 0.8 µm, this result is in good agreement with the expected value (28 µm).

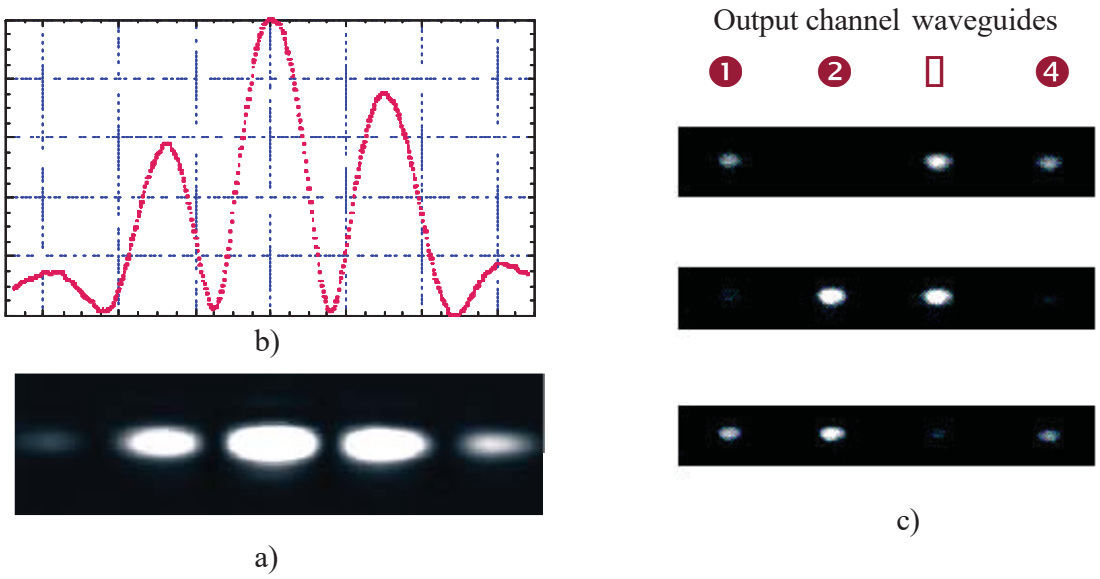

Fig. 7 : a) Photograph of the experimental interference pattern. b) intensity profile. c) intensity distribution in the four channel waveguides at the output of the interferometer for various phase differences between the two arms of the interferometer.

By inducing a path difference between the two arms of the interferometer, one can observe the variation of the intensity distribution collected in the four output waveguides of the sensor head (Fig. 7c).

The insertion losses of the interferometer head were measured as follow: a light beam coming from a fiber was injected in only one input arm of the interferometer and the intensity coupled in every output waveguide was measured. We obtained typical insertion losses of 9.5 dB in the central arms (2 and 3) and 14.5 dB in the lateral arms (1 and 4). The losses can be explained by the large lateral dimensions of the beam at the output of the planar waveguide.

4.5. characterization of the sensor head

After the fabrication of the device, a first characterization of the integrated sensor head is done in order to calculate the standard deviation of the intensity measurements with respect to the aimed values. According to the value of deviation, a post-annealing of the structure can be performed in order to balance the intensity distribution between the sensor arms.

Table 1 gives an example of intensity levels measured after adjustment of the component. The reference and measuring arms are excited separately in order to work in non- interferometric conditions.

The propagation losses of the buried waveguides are 0.2 dB/cm and the modefield mismatch between the channel waveguide and a circular fiber causes a fiber coupling loss of 0.8 dB. Taking into account the losses of the different elements of the structure, the estimated splitting ratio of the input coupler is 75 % (resp. 25%) in the measuring (resp. reference) arm of the sensor.

Table 1 shows a good balance between the two arms of the interferometers.

fibre	1000 µW
measuring arm	
output of the S bend (before lens 1)	390 µW
input of the measuring arm (after re-injection through lens 2)	195 µW
output of the photometric arm	6 µW
output of the central arms (2 or 3)	**15 µW**
output of the lateral arms (1 or 4)	**5 µW**
reference arm	
output of the central arms (2 or 3)	**18 µW**
output of the lateral arms (1 or 4)	**6.5 µW**

Table 1 : Intensity measurement results.

5. CONCLUSION

One main advantage of integrated optical interferometers is that the phase shift between the four output signals is determined only by the waveguide design of the structure (refractive index profile of the guide, angle between the tapers and separation distance of the output waveguides) and by the refractive index of the substrate. The creation of a one-dimensional fringe pattern coupled with four output waveguides allows a simple and precise multiphase detection.
We developed a double thermal exchange process adapted to the fabrication of guiding structures with large refractive index variation between the waveguide profile and the substrate. The strong confinement of the structure allows the fabrication of low losses integrated loop mirrors with bending radius as low as 10 mm. With the same process conditions, directional couplers and integrated interferometers were fabricated and characterized. A balanced integrated sensor head with relatively large output signals was tested. For a 1 mW signal in the fiber, the available signals before the photodetectors (in non-interferometer conditions of operation) are of the order of 16 µW (resp. 6 µW) in the central (resp. lateral) arms of the output waveguides.

ACKNOWLEDGMENTS
This work has been supported by CSO Mesure.

REFERENCES

[Fues 93] R. Fuest, N. Fabricius, U. Hollenbach, B. Wolf. “Interferometric displacement sensor realized with a planar 3*3 directional coupler in glass”. *Proceeding of the SPIE – The International Society for Optical Engineering* – vol. 1794, 1993, p. 352-365.

[Poup 00] A. Poupinet, L. Pujol, O. Sosnicki. “Spatialized interferometer in integrated optics” ICSO 2000.

[Scha 94] I. Schanen Duport, P. Benech, R. Rimet. “New integrated-optics interferometer in planar technology”. *Applied Optics*, vol. 33, n° 25, 1994, p. 5954-5958.

[Lang 98] T. Lang, D. Genon-Catalot, P. Dandrea, I. Schanen Duport, P. Benech. “Integrated optical displacement sensor with four quadrature phase shifted output signals”. *Journal of optics*, vol. 29, n°3, june 1998, p.135-140.

[Rama 94] R. V. Ramaswamy, R. Srivastava. “Ion-exchanged glass waveguides: a review”. *IEEE J. Ligthwave Technol*., vol. 6, 1994, p. 984-1002.